

A Radio Study of the Seyfert galaxy Markarian 6: Implications for Seyfert life-cycles

P. Kharb

*Centre for Imaging Science, Rochester Institute of Technology, 54 Lomb Memorial Drive,
Rochester, NY 14623*

kharb@cis.rit.edu

C. P. O' Dea

*Dept. of Physics, Rochester Institute of Technology, 84 Lomb Memorial Drive, Rochester,
NY 14623*

S. A. Baum

*Centre for Imaging Science, Rochester Institute of Technology, 54 Lomb Memorial Drive,
Rochester, NY 14623*

E. J. M. Colbert

*Johns Hopkins University, Dept. of Physics and Astronomy, 3400 North Charles Street,
Baltimore, MD 21218*

C. Xu

Space Telescope Science Institute, 3700 San Martin Drive, Baltimore, MD 21218

ABSTRACT

We have carried out an extensive radio study with the Very Large Array on the Seyfert 1.5 galaxy Mrk 6 and imaged a spectacular radio structure in the source. The radio emission occurs on three different spatial scales, from ~ 7.5 kpc bubbles to ~ 1.5 kpc bubbles lying nearly orthogonal to them and a ~ 1 kpc radio jet lying orthogonal to the kpc-scale bubble. To explain the complex morphology, we first consider a scenario in which the radio structures are the result of superwinds ejected by a nuclear starburst. However, recent Spitzer observations of Mrk 6 provide an upper limit to the star formation rate (SFR) of $\sim 5.5 M_{\odot} \text{ yr}^{-1}$, an estimate much lower than the SFR of $\sim 33 M_{\odot} \text{ yr}^{-1}$ derived assuming that the bubbles are a result of starburst winds energized by supernovae explosions. Thus,

a starburst alone cannot meet the energy requirements for the creation of the bubbles in Mrk 6. We show that a single plasmon model is energetically infeasible, and we argue that a jet-driven bubble model while energetically feasible does not produce the complex radio morphologies. Finally, we consider a model in which the complex radio structure is a result of an episodically-powered precessing jet that changes its orientation. This model is the most attractive as it can naturally explain the complex radio morphology, and is consistent with the energetics, the spectral index and the polarization structure. Radio emission in this scenario is a short-lived phenomenon in the lifetime of a Seyfert galaxy which results due to an accretion event.

Subject headings: galaxies: Seyfert — galaxies: individual (Mrk 6) — radio continuum: galaxies

1. INTRODUCTION

Radio observations show that most Seyfert galaxies have sub-parsec-scale radio emission (e.g., de Bruyn & Wilson 1976; Ulvestad & Wilson 1984a,b; Roy et al. 1994; Thean et al. 2000; Lal et al. 2004). Some of these galaxies with small-scale radio emission show elongated structures, similar to the radio jets seen in powerful radio galaxies. Radio emission on kiloparsec scales has also been detected in some Seyfert galaxies. The large-scale radio structures however are not typically found to be aligned with the small scale jets (Baum et al. 1993; Colbert et al. 1996; Gallimore et al. 2006). Further, Seyfert radio jets were found to be randomly aligned with respect to the host galaxy major axes (Kinney et al. 2000; Schmitt et al. 2001; Schmitt & Kinney 2002). Abrupt changes of jet axes were also found in some Seyfert galaxies, e.g., NGC 4151 (Ulvestad et al. 1998) and NGC 1068 (Gallimore et al. 1996). It appears that the radio structures in Seyfert galaxies are more complex than in the radio galaxies. Extensive discussions of large scale radio structures in Seyfert galaxies can be found in Baum et al. (1993); Colbert et al. (1996) and Gallimore et al. (2006).

Mrk 6 is an early-type (S0a) Seyfert 1.5 galaxy. It is also one of the Seyfert galaxies that have radio emission on both small and large scales. Using the Westerbork Synthesis Radio telescope (WSRT), Baum et al. (1993) detected a pair of large weak “radio lobes” extending northeast-southwest and a smaller scale radio structure extending east-west. High resolution MERLIN observations of the nuclear region by Kukula et al. (1996) revealed a well-defined jet extending in the north-south direction. This jet is nearly aligned with the ionization cone reported earlier by Meaburn et al. (1989), and the optical polarization position angle (P.A.) derived through spectropolarimetric observations (Smith et al. 2004). Kukula et al. (1996)

also found some evidence of a pair of lobes on the sides of the jet which corresponded to the east-west radio structure observed by Baum et al. (1993) and Nagar et al. (1999). However, due to the relatively poor resolution of WSRT ($\sim 3''.5$) and the limited u - v coverage of MERLIN, few conclusions could be made on the relation between the three scales of radio emission in this source. In order to have a better understanding of the radio structures in Mrk 6, we undertook a comprehensive radio study of Mrk 6 with the Very Large Array (VLA).

Throughout this paper we assume $H_0=71 \text{ km s}^{-1}\text{Mpc}^{-1}$, $\Omega_m = 0.27$ and $\Omega_{vac} = 0.73$. Therefore, at the redshift of $z=0.01881$ (recession velocity $\sim 5640 \text{ km sec}^{-1}$), or at the distance of 80.6 Mpc for Mrk 6, 1 arcsec is equivalent to 377 parsecs.

2. OBSERVATIONS AND DATA ANALYSIS

Mrk 6 was observed with the VLA at $\lambda 6 \text{ cm}$ (4860 MHz) and $\lambda 20 \text{ cm}$ (1430 MHz) during 1995–1996. Almost all VLA configurations were used in the observations in order to image Mrk 6 on different spatial scales. 3C 286 was used as the primary flux density and polarization calibrator, while 0614+607 was used as the phase calibrator for the entire experiment. The data were processed with NRAO’s software package AIPS using the standard imaging and self-calibration procedures. Table 1 lists the observing frequency, the corresponding bandwidth, the VLA configuration, the observation date, the FWHMs of the synthesized beams, the total flux densities of the source at various resolutions, and the *r.m.s.* noise in the final maps.

Table 1: Observation Log

Frequency (GHz)	BW (MHz)	Config.	Observation Date	Resolution (arcsec ²)	Total Flux Density (mJy)	r.m.s. (μ Jy/bm)
4.86	50	A	07/21/1995	0.41 \times 0.31	85.8	16
4.86	50	B	11/02/1995	1.43 \times 1.13	96.4	16
4.86	50	C	02/17/1996	4.27 \times 4.04	96.5	25
4.86	50	D	05/03/1995	16.2 \times 11.4	100.5	29
1.43	50	A	07/03/1995	1.44 \times 1.12	274.4	27
1.43	50	C	02/17/1996	13.9 \times 13.0	270.8	147
1.43	50	D	06/01/1995	59.1 \times 38.2	275.0	210

3. RESULTS

The total intensity radio maps are presented in Fig. 1 while Fig. 2 shows the relative orientation of the radio structures with respect to the extended emission-line region (ENLR) and host galaxy of Mrk 6. Figures 3 and 4 show the radio polarization and the spectral index images, respectively. We describe below the primary findings of our study.

3.1. Radio Morphology: Emission on Three Spatial Scales

Figure 1 displays the mosaic of radio emission at 6 cm. The radio map of the inner jets is from the MERLIN observations of Kukula et al. (1996). It is immediately apparent that Mrk 6 has radio emission on three scales. First, there is a radio jet of extent ~ 1 kpc ($3''$) extending in the north-south direction, at the active galactic nucleus (AGN). Second, there are a pair of inner bubbles of size $\sim 1.5 \times 1.5$ kpc ($\sim 4'' \times 4''$) each, extending east-west and nearly perpendicular to the central jets. And third, there are a pair of outer bubbles of dimensions $\sim 4.5 \times 7.5$ kpc ($\sim 12'' \times 20''$) each, extending northeast-southwest. In Fig. 2 we observe the relative orientation of these radio structures with respect to the extended [OIII] emission-line region as observed by Kukula et al. (1996) and the host galaxy optical continuum from the high-resolution HST image (obtained from the HST archive). We note that the inner kpc jet is roughly aligned with the emission-line gas. Further, the outer bubbles are aligned with the host galaxy minor axis. The SDSS image from the NASA/IPAC Extragalactic Database (NED) indicates that the extent of the galaxy is $> 15 \times 20$ kpc; the radio structures therefore lie within the confines of the host galaxy.

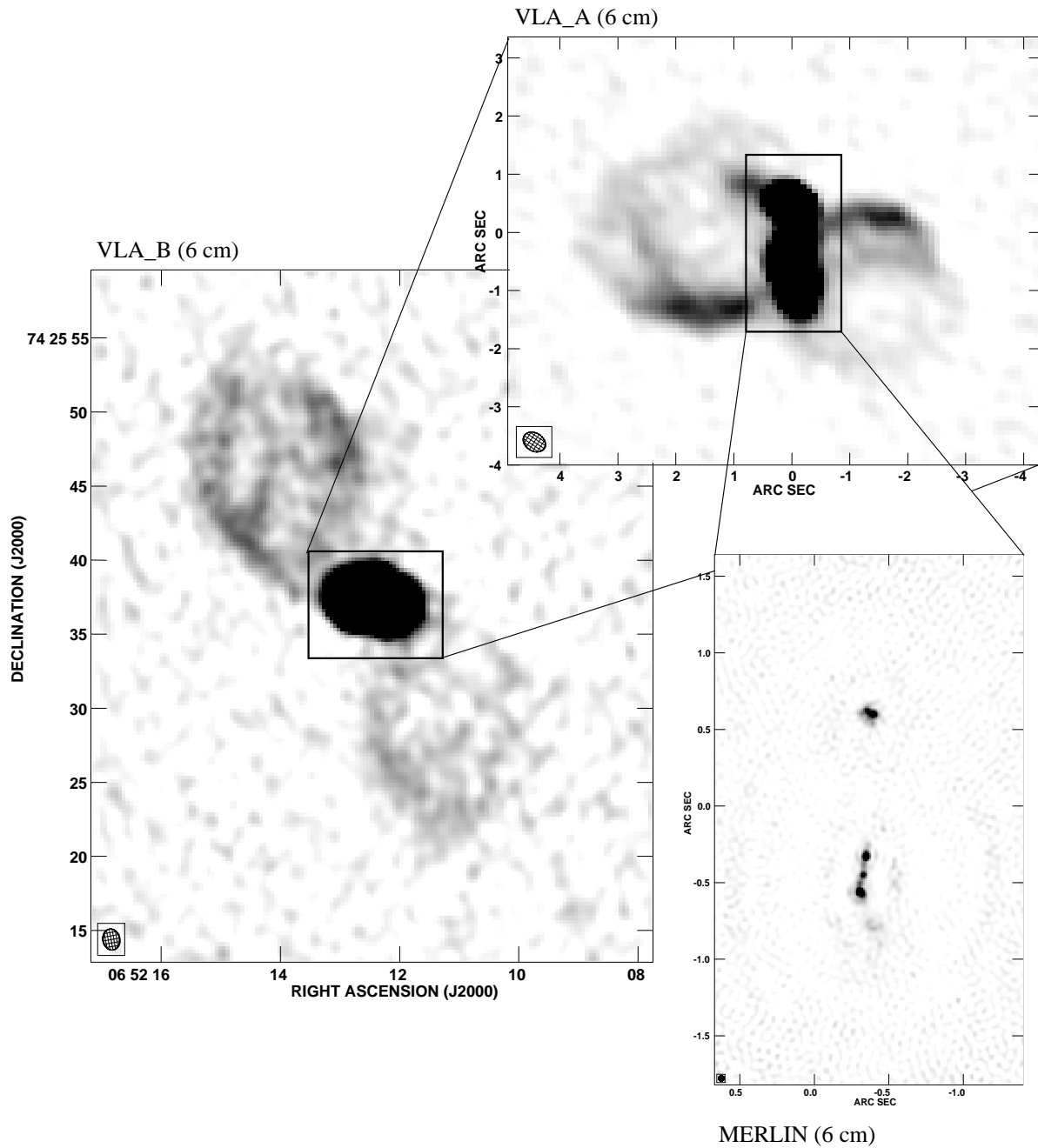


Fig. 1.— Grey scale images of the 6 cm radio structures observed in Mrk 6. The bubble-like structures are clearly seen in the VLA images. The MERLIN map of the inner jet is taken from Kukula et al. (1996). The centre of the optical host galaxy lies close to the (0,0) position in the MERLIN image, with a 3σ uncertainty of $0.27''$ (Clements 1981). There is no radio ‘core’ coincident with this position.

We have listed some geometric and physical parameters pertaining to these individual radio structures, including their sizes, position angles, flux density and spectral indices in Table 2. For the outer pair of bubbles, the radio flux density of the northeast bubble is about two and a half times that of the southwest bubble. For the inner pair, the radio flux density of the east bubble is about two times that of the west bubble. We note that (1) the two pairs of bubbles and the jets show self-similar characteristics in their morphologies and sizes, i.e., the width of the larger structure corresponds to the overall size of the next smaller structure, (2) the bubbles show clear edge-brightening and (3) the bubbles contain filamentary structures.

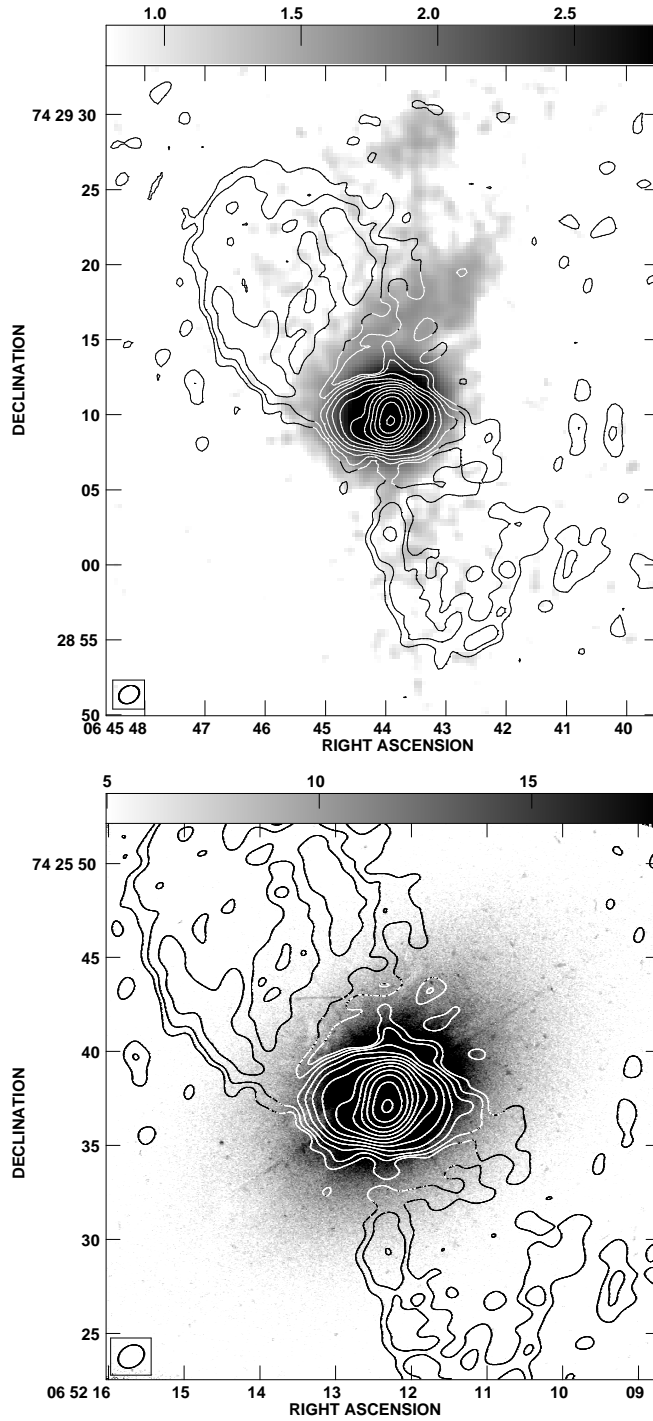


Fig. 2.— The 20 cm radio contours superimposed on the grey-scale images of (top) extended [OIII] emission-line region (Kukula et al. 1996), and (bottom) HST (WFPC2/F606W) optical continuum from the host galaxy (obtained from the HST archive). The outer bubble-like structures are projected roughly orthogonal to the major axis of the bulge-dominated S0a host galaxy. However, the structures lie within the extent of the host galaxy.

Table 2: Radio Properties of Mrk 6

Structure	Size (arcsec ²)	P.A.	S ₆ (mJy)	L ₆ (W Hz ⁻¹)	α_6^{20}
Jet	1×3	179°	75.0	5.8E22	-0.91±0.21
North	-0.90±0.14
South	-0.84±0.10
Inner Bubble	...	76°	11.4	8.9E21	...
East	4×4	...	7.9	6.1E21	-0.61±0.37
West	3×3	...	3.5	2.7E21	-0.55±0.30
Outer Bubble	-	33°	9.4	7.3E21	...
North	12×20	-	6.2	4.8E21	-0.71±0.21
South	12×18	-	3.2	2.5E21	-0.55±0.26

Note. — Col.2: Extents of structures using the 6 cm maps; Col.4: 6 cm flux density in mJy; Col.5: 6 cm luminosity in W Hz⁻¹; Col.6: Spectral index estimated using the 6 cm and 20 cm images.

3.2. Radio Polarization

Polarization was detected at 6 cm in the region corresponding to the western edge of the inner bubble and on the edges of the outer pair of bubbles. Figure 3 displays the 6 cm VLA C-configuration image with polarization electric vectors superimposed. The length of the vectors is proportional to the fractional polarization. At this configuration, polarization was detected at the 10–20 σ levels (or 0.2–0.4 mJy beam⁻¹). This corresponds to a high fractional polarization of $\sim 50\%$ at the edges and less than 1% polarization near the center.

We were unable to detect polarization on the edge of the outer bubbles with the B-configuration, and anywhere with A-configuration, due to the smaller beam size and lower resultant surface brightness sensitivity. A suitable taper on the B-configuration uv -coverage recovers the polarization features observed in the C-configuration image (Fig. 3), thus confirming the detection of polarization. Assuming that the radio emitting medium is optically thin, and the Faraday rotation is small at 6 cm (Galactic rotation measure is ≤ 30 rad m⁻² in the direction of Mrk 6, Simard-Normandin & Kronberg 1980), we infer the magnetic field orientation to be mostly aligned with the edge of the bubbles.

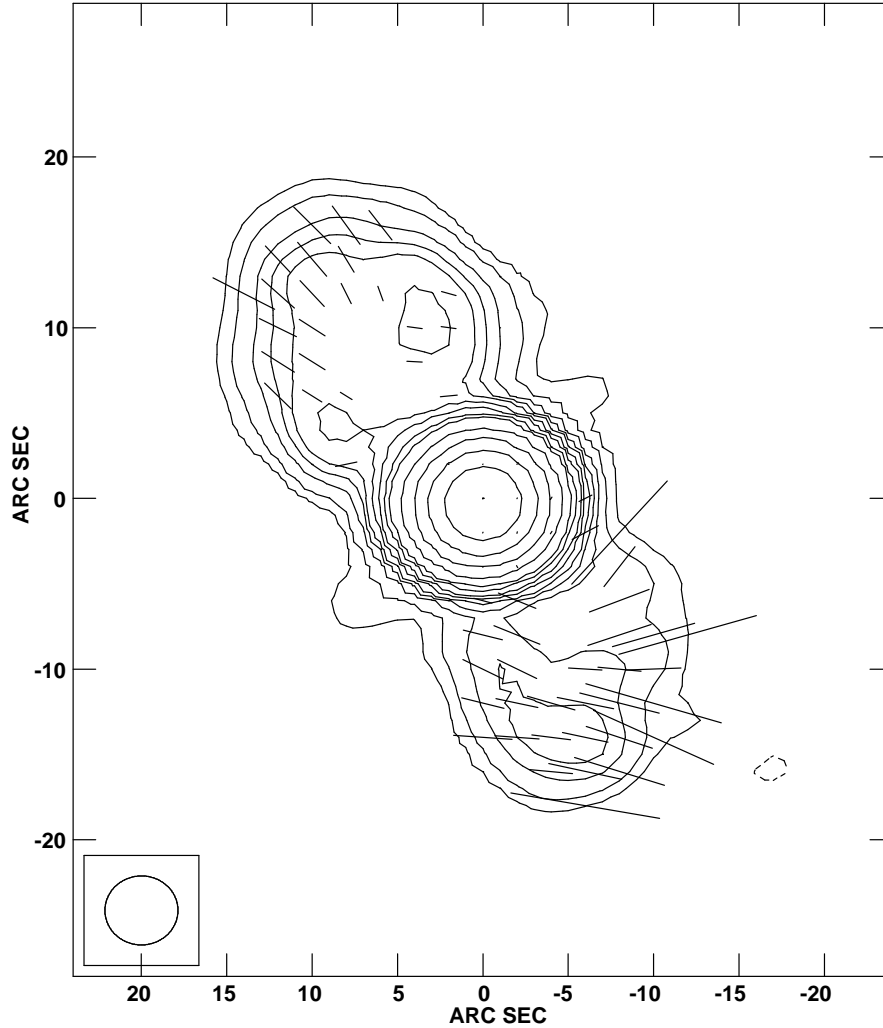


Fig. 3.— Contour image of Mrk 6 at 6 cm with polarization electric vectors and percentage of polarization indicated. The image was made using the VLA C-configuration data. The contour levels are $7.45 \times 10^{-5} \times (-1, 1, 2, 4, 6, 8, 12, 16, 24, 32, 64, 128, 256, 512)$ Jy/beam, with the beam size $4''.2 \times 4''.0$. The lowest contour level corresponds to 3 times the off source r.m.s noise. $1''$ in length of polarization vector corresponds to 10% of polarization.

3.3. Spectral Indices

Figure 4 (top) shows the 6 cm B-configuration contour image overlaid on the grey scale spectral index image, which was made from the 6 cm B-configuration and the 20 cm A-configuration images, after restoring both images with the same synthesized beam. The spectral indices vary only slightly across the image. The average spectral index over the central region corresponding to the inner bubbles is -0.78 ± 0.26 , that over the northern bubble is -0.71 ± 0.21 and that over the southern bubble is -0.55 ± 0.26 . These spectral indices are consistent given the large errors.

Figure 4 (bottom) displays the spectral index map between 6 cm and 18 cm, in the neighbourhood of the jets. This image was made by combining our 6 cm A-configuration map with the 18 cm MERLIN map from Kukula et al. (1996), at the matched resolution of $0''.4 \times 0''.4$. It shows that the spectral index of the northern hotspot in the jet is -0.90 ± 0.14 , that of the southern hotspot is -0.84 ± 0.10 and that of the saddle between the two hotspots is -0.96 ± 0.08 . Our results are in general agreement with those of Kukula et al. (1996). The average spectral index over the eastern bubble is -0.61 ± 0.37 and over the western bubble is -0.55 ± 0.30 , slightly flatter than those in the jets, but similar to those in the outer pair of bubbles.

3.4. Energetics

We have estimated the magnetic field strengths in regions corresponding to the bubbles assuming equipartition of energy between relativistic particles and the magnetic field (Burbridge 1959). Using Eqns. 1–5 of O’Dea & Owen (1987), we have also obtained the minimum pressure and particle energy (electrons and protons) at minimum pressure. These estimates are listed in Table 3. The averaged total radio luminosity (L_{rad}) was estimated assuming that the radio spectrum extends from 10 MHz to 10 GHz with a spectral index of $\alpha = -0.6$. Further, it was assumed that the relativistic protons and electrons have equal energies.

In Table 3 we list the minimum pressure values for the two scenarios where the bubbles are completely filled (volume filling factor, $\phi = 1$) or are mostly empty ($\phi = 10^{-3}$). The estimated minimum pressure in the filled outer bubbles turns out to be $\sim 10^{-12}$ dynes cm^{-2} and in the inner bubbles P_{min} is $\sim 10^{-11}$ dynes cm^{-2} . The pressure is about fifty times larger for the bubbles when the volume filling factor is $\phi = 10^{-3}$.

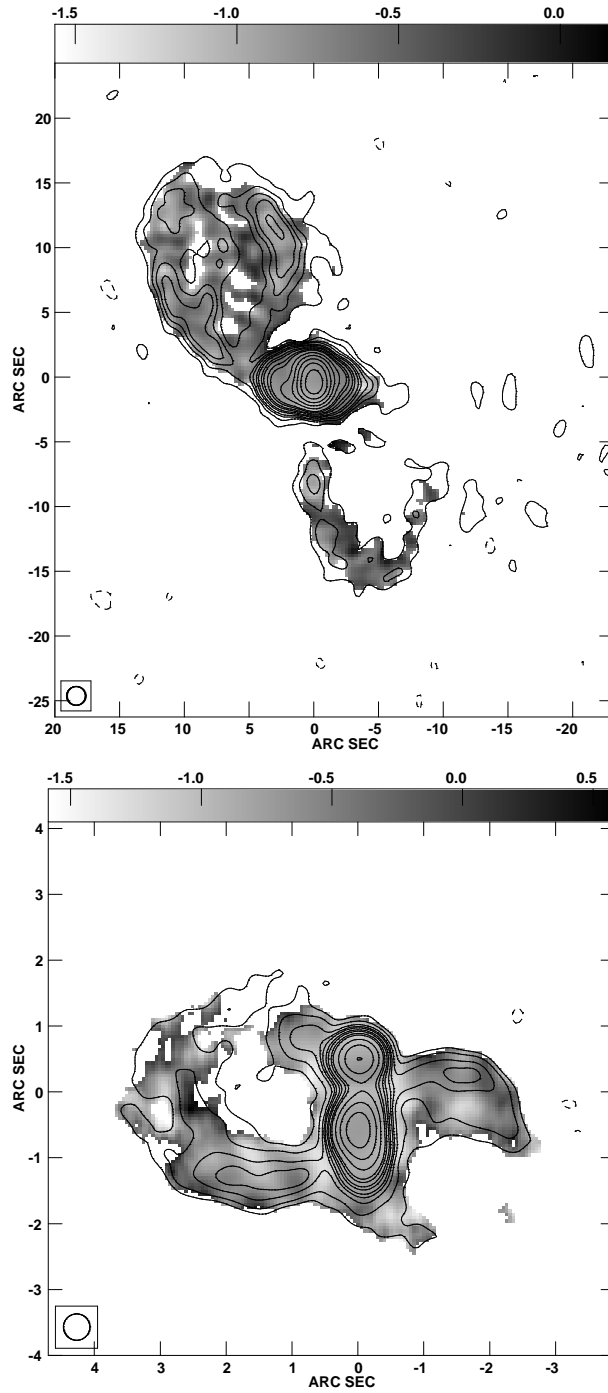


Fig. 4.— Spectral index map (see text) in greyscale overlaid on the (top) 20 cm A-configuration and (bottom) 6 cm A-configuration contour maps. The contour levels and beamsizes are (top) $8.82 \cdot 10^{-5} \times (-1,1,2,4,6,8,12,16,24,32,64,128,256,512)$ Jy/beam and $4''.5 \times 4''.5$ and (bottom) $7.0 \cdot 10^{-5} \times (-1,1,2,4,6,8,12,16,24,32,64,128,256,512)$ Jy/beam and $0''.5 \times 0''.5$.

4. DISCUSSION

Bubbles and rings have been observed in a few radio galaxies and quasars, for example, in Hercules A (Dreher & Feigelson 1984; Baum et al. 1996), 3C 310 (van Breugel & Fomalont 1984), and Centaurus A (Quillen et al. 2006). Bubble-like structures have also been observed in some Seyfert and starburst galaxies, e.g., NGC 2992, NGC 3079, NGC 5548, NGC 4051, and NGC 6764 (Wehrle & Morris 1988; Duric & Seaquist 1988; Baum et al. 1993; Nagar et al. 1999), and planetary nebulae such as η Carina and Hubble 5 (Nota et al. 1995; Dwarkadas & Balick 1998). Several mechanisms have been suggested for the formation of these bubble-like structures. We describe them in Sect. 4.2 and subsequently examine three potentially viable models for the formation of the radio structures in Mrk 6.

4.1. Constraints On A Model For Mrk 6

We note that the bubble-like structures observed in the above mentioned radio galaxies are essentially spherical and they are either part of or directly connected with the radio jet. This is different from the bubbles observed in Mrk 6 which are elongated, larger than the jet and not aligned with it. The elongated morphology of the bubbles make them more similar to the bubbles observed in planetary nebulae.

In order to estimate the originating point of the bubbles (where the two edges meet, see Fig. 5), under the simplifying assumption that the two edges of a bubble on either side lie in the same plane, we used a simple IDL program which, given the pixel positions of certain bright spots on the edges of the bubbles, fits a third degree polynomial to them, and derives the point where the difference in the position of the fitted functions is a minimum. Thus, it turns out that the outer pair of bubbles originate near $\alpha=06:52:12.359$, $\delta=+74:25:37.26$ (J2000) while the inner pair of bubbles originate near $\alpha=06:52:12.340$, $\delta=+74:25:37.081$ (J2000). Both originate from near the same place (offset by $0''.3$ or ~ 110 pc), which interestingly, lies around the hot spots 3 and 4 in Kukula et al. (1996) (to the south of the (0,0) position in the MERLIN image of Fig. 1). It should be pointed out that the bright spots we pick on the edges of the bubbles are not without ambiguities, which in turn give uncertain positions for the expected origins. The offset in the originating point of the bubbles may therefore not be of much significance. As Kukula et al. (1996) have noted, no radio ‘core’ has been found coincident with the centre of the optical host galaxy, which lies close to the (0,0) position (with a 3σ uncertainty in position of $0.27''$, Clements (1981)) in the MERLIN image (Fig. 1), and it is not clear if one of the knots $\sim 0.5''$ to the south, is the radio core.

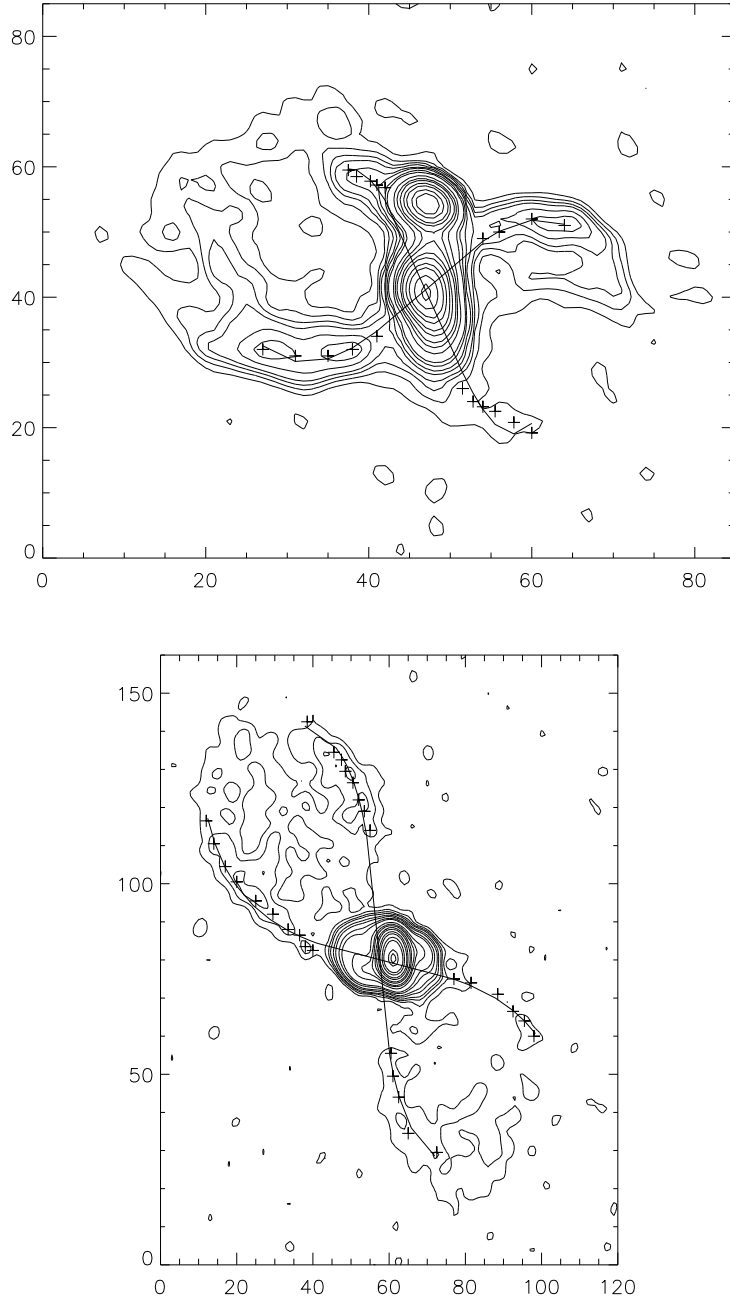


Fig. 5.— Extrapolations of bubbles down to their origins (see text). The axes coordinates are in pixels, the pixel size being $0.1''$ in the top and $0.25''$ in the bottom panel, respectively. This figure indicates that both pairs of bubbles originate from a region within 170 pc.

Table 3: Physical Properties and Energetics

Structure, Filling Factor (ϕ)	Length (")	Width (")	L_{rad} (erg s ⁻¹)	E_{min} (erg)	B_{min} (μ G)	P_{min} (dynes cm ²)
Outer Bubble, $\phi=1$						
North	20.4	12.1	7.4E38	9.7E54	3.6	1.2E-12
South	17.8	12.4	3.8E38	6.4E54	3.0	8.7E-13
Inner Bubble, $\phi=1$						
East	3.8	3.7	9.4e38	2.0E54	12.3	1.4E-11
West	3.0	3.2	4.2e38	9.9E53	11.3	1.2E-11
Outer Bubble, $\phi=10^{-3}$						
North	7.4E38	5.1E53	25.9	6.2E-11
South	3.8E38	3.3E53	22.0	4.5E-11
Inner Bubble, $\phi=10^{-3}$						
East	9.4E38	1.0E53	88.4	7.2E-10
West	4.2E38	5.1E52	81.4	6.1E-10
North-South Jet						
Outer Jet (North)	3.1	1.0	9.0E39	2.1E54	52.3	2.5E-10
	6.8	3.0	1.3E38	6.9E53	6.7	4.1E-12
	7.5	3.1	1.5E38	8.1E53	6.7	4.1E-12
Outer Jet (South)	7.2	3.1	8.7E37	5.7E53	5.7	3.0E-12
	5.4	2.0	3.6E37	2.1E53	6.2	3.6E-12
Inner Jet (East)	1.8	0.8	3.5E38	2.2E53	27.4	6.9E-11
	1.5	0.7	7.3E37	7.4E52	19.9	3.7E-11
Inner Jet (West)	1.4	0.6	3.2E37	3.9E52	17.6	2.9E-11
	1.5	0.7	1.8E38	1.2E53	25.8	6.2E-11

Note. — Col.2 and Col.3: The length and width in arcsecs of the volume element considered for the calculations, using the 6 cm image. L_{rad} = averaged total radio luminosity (see Sect. 3.4), E_{min} and B_{min} correspond to the particle energy and magnetic field strength at the minimum pressure P_{min} , obtained assuming the ‘equipartition’ condition. The upper part of the table has the parameters listed for the bubbles which are either completely filled ($\phi=1$) or mostly empty ($\phi=10^{-3}$), while the lower part of the table lists the parameters for the radio jet and volume elements taken along the edges of the bubbles, assuming $\phi=1$. In the precessing jet scenario, these volume elements correspond to portions of the precessing radio synchrotron jet. Outer Jet (North) corresponds to a volume element taken along the edge of the northern outer bubble on either side, and so on.

4.2. Mechanisms for Producing Bubble-like Structures

Extended radio structures have been observed in both Seyfert and starburst galaxies, and some of the structures are bubble-like (Colbert et al. 1996; Heckman et al. 1993). In starburst galaxies, the bubble-like radio structures have been suggested to form through the interaction between the starburst superwind and the ISM (Duric & Seaquist 1988; Heckman et al. 1993). In the case of Seyfert galaxies, Colbert et al. (1996) found that the kpc-scale radio outflows are more consistent with diverted AGN-driven jets. But they didn’t rule out the possibility that the outflows are starburst superwinds. In fact, indications of both AGN and starburst activity have been found in Seyfert galaxies like NGC 7469 (Genzel et al. 1995), NGC 3079 (Veilleux et al. 1994) and the Circinus galaxy (Maiolino et al. 1998).

Other scenarios have been proposed to explain bubble formation in galaxies. In order to explain the spherical shell-like structures in the radio galaxies Her A and 3C 310, Morrison & Sadun (1996) introduced a model wherein acoustic waves or weak shocks are excited along the jet axis of the AGN, in a pre-existing thermal galactic wind. These acoustic shells expand uniformly at the speed of sound and drift along with the wind. At a much later second stage, a new and much faster flow of relativistic plasma is energized by the AGN, which fills these shells with radio-emitting electrons, thus creating radio-bright bubbles. Alternately, Pedlar et al. (1985) invoked a model of expanding radio-emitting plasmons which shock, compress and accelerate the forbidden-line gas in Seyfert galaxies. Both these models require the bubbles to be continuously injected with relativistic particles from the AGN.

Bubble-like structures observed in some planetary nebulae like Hb 5, (Terzian & Hajian 2000)¹ or η Carina (Nota et al. 1995), have been suggested to arise due to the presence of orbiting binary companions (Soker 2004). A binary black hole system could similarly be invoked to explain the bubble-like structures in Mrk 6. In this picture, the primary black hole is spinning and is responsible for the formation of the radio jet. The secondary black hole on the other hand, is not spinning but orbits the primary black hole in a plane which is perpendicular to the inner bubbles. The quasi-spherical disk wind from the primary black hole forms an accretion disk around the secondary black hole. This in turn launches fast winds into the pre-existing “density contrast” between the equatorial and polar directions (see Balick 1987) created by the orbiting secondary black hole.

The complexity involved in this binary blackhole model with the two blackholes having perpendicular orbital planes, however, makes it unattractive. For example, the orbital plane of the secondary black hole will be aligned with the inner jet axis and must exert a

¹<http://ad.usno.navy.mil/pne/gallery.html>

disturbing influence on its propagation (Merritt & Milosavljević 2005), an effect which is not observed in the high resolution MERLIN image. Further, the existence of a secondary black hole orbiting in a plane perpendicular to the accretion disk of the primary, must have discernable effects (Sillanpaa et al. 1988; Lehto & Valtonen 1996) on the dynamics of the 100 pc-scale disk (Gallimore et al. 1998) which we assume to be relatively stable according to the ENLR (Meaburn et al. 1989, see Fig. 2), and the optical polarization position angle derived through spectropolarimetric observations (Smith et al. 2004). It is also uncertain whether the planetary nebula model will scale to an AGN. In the following sections, we discuss in some detail the pros and cons of three potentially viable scenarios that could give rise to the bubble-like structures in Mrk 6, *viz.*, (i) a starburst-driven bubble scenario, (ii) a jet-driven bubble scenario, and (iii) a precessing jet scenario.

4.2.1. Starburst-driven Bubble Scenario

The morphology of the pairs of the bubbles, especially their edge-brightening suggests that the radio emission could come from the shells of superbubbles. The sharp and well-defined edges of the bubbles and the existence of filaments in the bubbles would be consistent with strong interaction between the bubbles and the interstellar medium (ISM) where the radio-emitting particles (relativistic electrons) are accelerated and/or the magnetic field gets amplified (Pacholczyk & Scott 1976). For example, if the expansion of the bubbles are caused by diffusion with little interaction (shocks), we would expect the bubbles to be more irregular and diffusive, as seen in most radio lobes. The spectral index of the bubbles seems rather flat, also consistent with interaction and particle re-acceleration.

Assuming that the outer bubbles are formed through starburst winds energized by supernovae explosions, we estimate the energy budget. If we assume the bubbles are filled with the ejecta from the supernovae, the energy required for the bubbles to expand to the present sizes ($V \sim 7.5 \times 4.5 \times 4.5 \text{ kpc}^3$) adiabatically within the ISM of pressure $P \sim 10^{-10} \text{ dynes cm}^{-2}$ is $4PV = 1.7 \times 10^{57} \text{ ergs}$. This corresponds to 1.7×10^6 supernova explosions with individual explosive energy of 10^{51} ergs . For wind speeds of 1000 km s^{-1} , the time required for the bubbles to expand to the present size is $\sim 7 \times 10^6 \text{ yrs}$. Thus the required supernova explosion rate is $\sim 0.24 \text{ yr}^{-1}$, which is comparable to the predicted rate for the prototypical starburst galaxy M 82 (Seaquist & Odegard 1991; Rieke et al. 1993). The required supernova rate would be reduced if the bubbles are not fully filled with the superwinds. We must mention that we have not included the loss through radio emission since it is negligible compared with the dynamical energy we have estimated above.

The derived supernova rate can yield an estimate of the required star-formation rate

(SFR). By assuming a Salpeter initial mass function over the mass range $0.1 \leq M/M_{\odot} \leq 100$, using the above derived supernova rate, we obtain (by using Eqns. 28, Condon et al. (2002) and 20, Condon (1992)), a large star-formation rate of $\sim 33 M_{\odot} \text{ yr}^{-1}$ for Mrk 6. The SFR estimated from the 1.4 GHz luminosity of the bubbles ($\sim 6 \times 10^{22} \text{ W Hz}^{-1}$) for $\alpha = -0.6$ and Eqns. 21 of Condon (1992) and 28 of Condon et al. (2002), turns out to be much larger (SFR $\sim 76 M_{\odot} \text{ yr}^{-1}$).

An upper limit to the SFR can be obtained from recent Spitzer IRAC observations of Mrk 6 (Buchanan et al. 2006). Using the $8\mu\text{m}$ flux density of 0.1 Jy resulting from the central $\sim 7''$ region (corresponding to a spatial scale of 2.7 kpc), and the relation, $\text{SFR} = 2.0 \times 10^{-43} \nu L_{\nu}(8 \mu\text{m}) \text{ erg sec}^{-1}$, (Calzetti et al. 2006, in prep.), which makes use of the nebular lines calibration of Kennicutt (1998), we obtain a SFR ($M \geq 0.1 M_{\odot}$) $\sim 5.5 M_{\odot} \text{ yr}^{-1}$. This value is much lower than the SFR derived assuming that the bubbles are a result of starburst winds energized by supernovae explosions.

The derived minimum pressure estimate for the bubbles ($\sim 10^{-11} - 10^{-12} \text{ dynes cm}^{-2}$) is one to two orders of magnitude lower than the typical ISM pressure of $\sim 10^{-10} \text{ dynes cm}^{-2}$ found in an elliptical or an S0 galaxy (Mathews & Brighenti 2003). This could imply that either (i) the pressure has a large contribution from thermal particles, (ii) the equipartition condition does not exist in the bubbles, or (iii) the equipartition condition exists and the derived pressure estimates are the actual ISM pressures in Mrk 6. Further, through optical spectroscopic observations, Heckman et al. (1990) have found typical kpc-scale pressures of $2 - 4 \times 10^{-9} \text{ dynes cm}^{-2}$, in a sample of galaxies with starburst-driven galactic superwinds. The derived P_{min} values for Mrk 6 are two to three orders of magnitude lower (see Table 3). If we assumed that the bubbles were powered by superwinds, then this low P_{min} could imply that there is a large thermal contribution to the pressure, or the equipartition condition does not hold, or the bubbles are not powered by typical superwinds. In their work on the X-ray binary SS433, Blundell et al. (2001) have suggested that powerful accretion disk winds, which arise perpendicular to the radio jet, can also contribute to the radio luminosity. An accretion disk outflow cannot be ruled out in Mrk 6.

In summary, the superwind model has the advantage that the complex geometry of the radio emission and the different features can be understood as being determined by their own local environments. The disadvantage of the model is that it cannot explain the similarities between the two pairs of the bubbles, if the similarities are not simple coincidences. However, the most important concern for this model stems from the derived energetics – the upper limit to the SFR provided by Spitzer observations indicates that a starburst alone cannot meet the energy requirements for the creation of the bubbles in Mrk 6.

4.2.2. AGN-driven Bubble Scenario

The distorted appearance of many Seyfert jets has led to the suggestion that the jet diverts due to interaction with molecular gas, within the central hundred parsecs (e.g., Gallimore et al. 1996; Bicknell et al. 1998; Gallimore et al. 2006). The jet eventually terminates in a bow shock which plows into the surrounding ISM, resulting in bow-shock-like structures on kiloparsec scales, similar to the structures observed in Mrk 6. Assuming that the efficiency (ϵ) with which the total jet energy is tapped to produce radio luminosity is 1% (see for e.g. O’Dea 1985), the jet with a radio luminosity of $\sim 10^{40}$ ergs sec $^{-1}$ (see Table 3), and a kinetic luminosity ($\frac{L_{\text{rad}}}{\epsilon}$) of $\sim 10^{42}$ ergs sec $^{-1}$, would require $\sim 3 \times 10^5$ years to deposit all its energy into the nuclear ISM and produce the derived minimum energy of $\sim 10^{55}$ ergs for the outer bubble. The jet would require only $\sim 7 \times 10^4$ years to produce the derived minimum energy for the inner bubble. Although this model seems energetically feasible it does not naturally explain the two edge-brightened nested radio structures or the fact that the inner jet is perpendicular to the inner set of bubbles.

We note that the pressure-volume energy of the outer bubble is around a hundred times larger than the derived minimum energy. Therefore, if the equipartition condition holds, the energy contribution from the thermal particles to the bubbles, must be a hundred times greater than from the relativistic electrons.

AGN-driven plasmons have also been proposed to explain bubble-like structures in Seyfert galaxies (Pedlar et al. 1985). Models of radio emission from idealized plasmons (e.g., Shklovskii 1960) suffer severe adiabatic losses resulting in their radio luminosity decreasing as r^{-5} , where r is the radius of the plasmon. Assuming adiabatic losses in a spherically expanding radio plasmon of relativistic gas, the final luminosity and internal energy of the plasmon is given by $L = L_0(r_0/r)^5$ and $E = E_0(r_0/r)$, respectively, where L_0 and E_0 are the initial luminosity and internal energy of the plasmon with initial radius r_0 . Using $L = 7.4 \times 10^{38}$ ergs sec $^{-1}$ and $E = 5 \times 10^{53}$ ergs at a radius $r=7.5/2=3.75$ kpc for the outer bubble (see Table 3 for $\phi = 10^{-3}$), we derive a large initial luminosity and internal energy of $L_0 \sim 6 \times 10^{56}$ ergs sec $^{-1}$ and $E_0 \sim 2 \times 10^{57}$ ergs, at the radius $r_0=1$ pc. Similarly for the inner bubble with $r=3.8/2=1.9$ kpc, we derive $L_0 \sim 2 \times 10^{55}$ ergs sec $^{-1}$ and $E_0 \sim 2 \times 10^{56}$ ergs, at $r_0=1$ pc. However, typical bolometric luminosities for Seyferts galaxies fall in the range of $10^{45} - 10^{46}$ ergs sec $^{-1}$ (Padovani & Rafanelli 1988), making the L_0 estimate unreasonable. Alternatively, an energy equivalent of 10^5 years of bolometric luminosity must be released at the radio frequency alone, at one instant. A single plasmon model for the bubbles of Mrk 6 therefore seems to be energetically implausible.

4.2.3. Precessing Jet Scenario

In this model, an episodic precessing jet is the prime mover that has produced all of the radio structure visible in Mrk 6. Assuming a jet velocity of $\sim 10^4$ km s $^{-1}$ (Bicknell et al. 1998; Ulvestad et al. 1999), and the bubbles-edges to be a precessing jet, the outer bubbles would have resulted in $\geq 7 \times 10^5$ years and the inner bubbles would need $\geq 1 \times 10^5$ years to form. The gap between the size-scales of the two pair of bubbles would imply different episodes of ejection separated by $\geq 6 \times 10^5$ years. Therefore, the outer bubbles would be the relic of the radio jet emission from about 10^6 years ago as it precessed in the northeast-southwest direction, probably following an accretion event. The precessing jet subsequently changed direction and pointed in the east-west direction about 10^5 years ago, possibly following another accretion/ejection episode. If the jet velocity is closer to 10^3 km s $^{-1}$ (e.g., Whittle et al. 2004), the time-scales for the formation of the outer and inner “bubbles” would be $\geq 7 \times 10^6$ years and $\geq 1 \times 10^6$ years, respectively.

With this picture in mind, we derived the proper motions of two precessing jets with $\beta = 0.03$, corresponding to the two phases of activity of the AGN, using Eqns. 1–4 of Hjellming & Johnston (1981). In Figure 6, we have plotted the proper motions of the precessing jet projected on the sky (i.e., the μ_α and μ_δ parameters as described in Hjellming & Johnston, 1981), for two different jet inclinations and precession cone opening angles. The parameters pertaining to this model are listed in Table 4. The model suggests that the northern outer and the eastern inner jets are approaching jets (denoted by solid lines in Fig. 6), while the southern outer and the western inner jets are receding jets (denoted by dashed lines in Fig. 6). Further, the outer jets precess in the clockwise sense, while the inner jets precess in the counterclockwise sense. The jet flips its axis by ~ 140 degrees between the two epochs.

The similarity between the precessing jet model and the radio images is striking. In the model, assuming only adiabatic losses and minimal radiative losses in the radio emitting plasma, the right edge of the northern outer “bubble” and the left edge of the southern outer “bubble” would both be brighter and have a flatter spectral index, as it would correspond to the most recent position of the jet. Elsewhere the spectra would have steepened due to the loss of energy in the synchrotron-emitting particles. The same would apply to the bottom edge of the eastern inner “bubble” and the top edge of the western outer “bubble”. As we see in Fig. 6 and Fig. 4, this is in good agreement with the observations. Further, the precession model easily reproduces the elongated morphology of the outer bubbles and the north-south S-shaped MERLIN jet – it is the projected terminal position of the jet that formed the inner “bubble” structure.

The precessing jet model yields precession periods of 3×10^6 and 4×10^5 years for the

outer and inner jets, respectively (Table 4). Further, the jets were “on” for approximately one precession period in each episode of activity. The similarity in the precession and the “activity” period is perhaps suggestive of a link between the two phenomena – the accretion event itself could be the cause of the precession. It is very interesting that Natarajan & Pringle (1998) find the timescale for the accretion disk/blackhole alignment for a $10^6 - 10^7 M_\odot$ blackhole (see for example Peterson et al. 2004, for Seyfert blackhole estimates) accreting at one-tenth of the Eddington limit, to be of the order of $6 - 7 \times 10^5$ years.

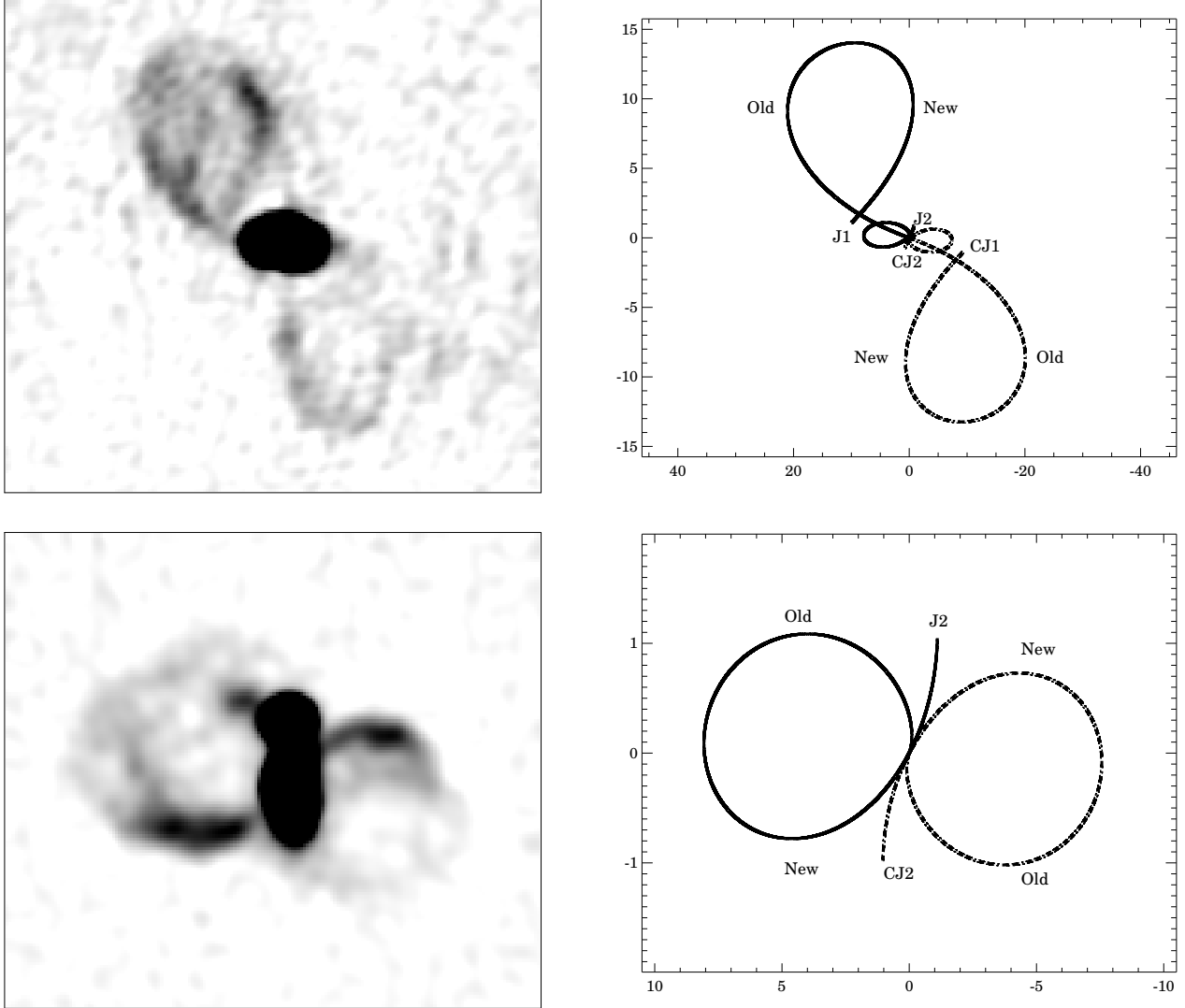


Fig. 6.— A comparison of the morphology of an episodically-powered precessing jet (top right) and the 20 cm radio image (top left). (Right) Plots of the proper motions of the precessing jet projected on the sky (i.e., the μ_α and μ_δ parameters as described in Hjellming & Johnston, 1981). The axes are in arcseconds, the solid line represents the approaching jet, while the dashed line represents the receding jet. The outer and inner “bubbles” are jets from two different phases of activity of the AGN. J1, CJ1, J2 and CJ2 indicate the jet and counterjet from the two phases and their approximate end-positions. In the precession model, the right edge of the northern outer bubble and the left edge of the southern outer bubble (both marked “New”) would be brighter and have a flatter spectral index, as it corresponds to the most recent position of the jet. The same applies to the bottom edge of the eastern inner bubble and the top edge of the western outer bubble (bottom panel). This agrees with the image on the left. Finally, the S-shaped MERLIN jet is easily reproduced in this model.

Table 4: Precessing jet parameters

Structure	i	ψ	χ	β	P	t
	(deg)	(deg)	(deg)		(yr)	(yr)
(1)	(2)	(3)	(4)	(5)	(6)	(7)
Outer jet	153	24	-30	0.03	3×10^6	1.7×10^6
Inner jet	9	9	-30	0.03	4×10^5	4×10^5

Note. — Col.1: In the precessing jet model, the outer and inner jets correspond to the the outer and inner “bubbles” in Mrk 6, Col.2: Inclination angle of the jet axis, Col.3: Half-opening angle of the precession cone, Col.4: Angle needed to rotate the geometrical model so that the axes coincide with the true north and east (see Hjellming & Johnston 1981), Col.5: Jet speed with respect to speed of light, Col.6: Precession period in years, Col.7: Total time the jet was “on” in years, assuming the jet speed given in Col.5. The jet sign parameter, $s_{jet} = +1$ was used for the approaching northern jet and $s_{jet} = -1$ for the receding southern jet. The rotation sign parameter, $s_{rot} = -1$ was used to imply clockwise motion of the precessing outer jet while $s_{rot} = +1$ was used for the counterclockwise precessing inner jet.

In order to test the precession model, we derived a spectral age using the difference in the spectral index values taken from the two opposite edges of the eastern inner “bubble” (marked ‘New’ and ‘Old’ in Fig. 6, bottom right), under the assumption that the spectral steepening is a result of ageing. Using the Jaffe & Perola (1973) model for spectral ageing and following the analysis described in Myers & Spangler (1985), we derived a radiative age of 4×10^5 years, assuming an equipartition magnetic field of $\sim 90 \mu\text{G}$ (Table 3). This estimate is a good match to the timescale the inner jet was “on” in the precessing jet model, providing further support to the model.

The fractional polarization values along the edges of the bubbles range from 20% to 40%, values that are typically observed in AGN jets. Typical values for the measured polarization of supernova remnants, on the other hand, are less than 10% on all scales (eg., Gaensler & Wallace 2003; Lazendic et al. 2004; McConnell et al. 2006). The polarized emission indicates that the southern side of the outer and the western side of the inner bubbles is more polarized than the opposite sides. However, the radio polarization seems to be anticorrelated with the presence of the emission-line gas (see Kukula et al. 1996), suggestive of depolarization of the northern and eastern bubble by ionized gas. Such an anticorrelation has also been observed in some radio galaxies (Heckman et al. 1982; Liu & Pooley 1991). We have estimated P_{min} for volume elements along the edges of the bubbles, assuming a volume filling factor of unity (see Table 3). In the precessing jet scenario, these correspond to sections of the radio synchrotron jet. We find the minimum pressure to be $\sim 3 - 6 \times 10^{-11}$ dynes cm^{-2} and the minimum pressure magnetic field to be $\sim 16 - 26 \mu\text{G}$ for sections of the inner bubble edge. The minimum pressure and magnetic field strengths are lower by an order of magnitude in portions of the outer bubble edge. We find that these values are similar to those obtained for radio jets in radio galaxies (Bridle et al. 1981; Bridle & Perley 1984) and Seyferts (e.g., Pedlar et al. 1985).

The 6 cm MERLIN image of Mrk 6 reveals a gentle S-shaped knotty radio source (easily reproduced in our precession model, see Fig. 6) which has often been suggested to be the signature of a precessing jet. Episodic ejection of material into a two-sided, precessing (or wobbling), collimated outflow or jet has been proposed to explain the point-symmetric morphology of planetary nebulae (Livio & Pringle 1997; Raga et al. 1993; Lopez et al. 1993; Soker & Livio 1994; Livio & Pringle 1996). Specific examples include the pre-planetary nebulae IRAS 16342-3814 (Sahai et al. 2005) and Hen 3-1475 (Velázquez et al. 2004), the planetary nebulae K3-35 (Miranda et al. 2001) and M2-9 (Schwarz & Monteiro 2004), the AGB star W43A (Imai et al. 2002), the symbiotic star CH Cygni (Crocker et al. 2002) and Herbig-Haro type jets (Lim 2001).

The S-shaped symmetry in jets has been observed in Seyfert galaxies like Mrk 3,

NGC 4151, NGC 5256, NGC 2685 and radio galaxies like 3C 305, 3C 345, 3C 294, 3C 334, and 3C 120 (Kukula et al. 1993; Pedlar et al. 1993; Heckman et al. 1982; Caproni & Abraham 2004b; Caproni et al. 2004). Most Seyfert galaxies observed on arcsecond-scales, do not show extended jets (e.g. Nagar et al. 1999). However when jet-like features are observed, they more often than not, exhibit a curved geometry (e.g. Ulvestad & Wilson 1984b; Kukula et al. 1995; Nagar et al. 1999; Thean et al. 2000). Indeed, 8 or S-shaped radio structures, sometimes along with large misalignments between radio structures on different spatial scales have been observed in the Seyfert galaxies NGC 2992, NGC 3079, NGC 5548, NGC 4051, NGC 6764, NGC 2110, NGC 4151, NGC 7469 (Wehrle & Morris 1988; Duric & Seaquist 1988; Baum et al. 1993; Nagar et al. 1999; Thean et al. 2001).

Further support for the precessing jet model comes from the emission line images obtained with the Hubble Space Telescope (Capetti et al. 1995), where the [OIII] and [OII] emission of Mrk 6 follows the curve of the S-shaped jet far into the southern edge of the inner bubble. It would be difficult to explain this asymmetry in emission-line morphology with an expanding shell of starburst superwinds. The entire narrow-line region itself extends much beyond the extent of the radio source. A similar curvature in the narrow-line region and an ENLR much larger than the radio source have been observed in the Seyfert 2 galaxy, Mrk 3 (Kukula et al. 1993) and the radio galaxy 3C 305 (Heckman et al. 1982). Similar to the suggestions made for these galaxies (see Kukula et al. 1993), we interpret that the small-scale emission-line region is powered by the radio jets while the ENLR may be ionized by the radiation from the nucleus. However, in keeping with the picture of an episodic precessing jet, it is possible that some of the emission in the ENLR is a result of an earlier interaction with the radio jet.

Therefore, based on all the above findings, we believe that the complex radio morphology of Mrk 6 can be understood in terms of an episodically-powered precessing jet. Mrk 6 may therefore be a unique object only in the sense that we are able to observe the source in its short-lived phase of episodic activity and before its radio emission from the previous epoch has faded away. Hence, similar radio structures may be found in other Seyfert galaxies going through such a phase, and when they are observed with sufficient resolution and sensitivity to image the relic emission from an earlier phase of activity.

4.2.4. Implications of an Episodic Precessing Jet

An episodically-powered precessing jet model in Seyfert galaxies implies that radio activity is a short-lived phenomenon in the lifetime of a Seyfert galaxy. Further, multiple episodes of ejection are possible. These might be caused by independent accretion events. Based on

the fraction of spiral galaxies which are Seyferts, Sanders (1984) estimated the statistical Seyfert lifetime to be of the order of $3 - 7 \times 10^8$ yrs. Further, based on the physical extents of the narrow emission line regions and radio jets, Sanders concluded that Seyfert nuclear activity must be short-lived stochastic accretion events with no single episode lasting longer than 10^6 yrs. Although the estimate of the fraction of Seyferts in spirals has increased from a few percent to $\sim 10\%$ following more recent surveys (Ho et al. 1997), thereby increasing the statistical lifetime to 10^9 yrs, the episode lifetime remains the same. Random jet orientations in Seyferts occur, in his picture, because each accretion event is accompanied by its own independent accretion disk in no preferred plane. Based on the NICMOS imaging of a large sample of Seyfert galaxies, Hunt & Malkan (2004) also reached the conclusion that Seyfert activity may be prompted by a disturbance.

The precessing jet model further implies that the jet ejection axis is easily perturbed in Seyferts. An accretion disk which is irradiated by a central AGN can become unstable to becoming warped, resulting in the wobbling of the jet (Pringle 1996, 1997; Livio & Pringle 1997) and severe misalignment of the jet axis and the axis of the outer accretion disk. Apart from radiative feedback that may warp a rotating accretion disk, jet precession could arise due to near-Eddington accretion events that may alter the spin of the supermassive black hole, in turn affecting the orientation of the radio jet (Rees 1978; Scheuer & Feiler 1996; Natarajan & Pringle 1998); binary blackholes (Caproni & Abraham 2004a) and blackhole mergers, that might result in short timescale redirection of the jet axis (Merritt & Ekers 2002; Merritt & Milosavljević 2005). Possibly due to the smaller blackhole masses in Seyfert galaxies compared to typical radio galaxies (e.g., McLure & Dunlop 2001), the spinning blackhole axis and consequently the radio jet axis is perturbed easily when accretion events take place, resulting in precessing jets and switches in jet-orientation.

It must be noted that the host galaxy of Mrk 6 shows no conspicuous signatures of galaxy-galaxy interaction or merger-activity, which could lead to a binary black hole in the centre (e.g., Begelman et al. 1980). In fact, Mrk 6 seems to be located in a sparse environment (Dahari 1985; Pfefferkorn et al. 2001), although the possibility of a major merger more than a dynamical timescale ($\sim 10^9$ yrs) ago, cannot be ruled out. Note that the emission-line region in Mrk 6 is extended along more than one axis (Fig. 2). However, as Dennett-Thorpe et al. (2002) point out from their study on ‘winged’ radio galaxies, there remain two possibilities that could result in jet realignment without a second black hole. (1) An ingested dwarf galaxy may not leave observable traces that a larger merger would, and yet provide adequate mass and angular momentum to cause jet re-orientation. (2) The jet axis may not be determined by the black hole alignment, but be strongly influenced by the accretion disk. Instabilities in the inner disk could then cause switching of the jet direction over short timescales.

A consequence of the changes in jet orientation is that the jet may interact with the molecular torus, stirring up the constituent matter. This would be consistent with the variable absorbing gas column density inferred through XMM-Newton X-ray spectroscopic observations of the central regions of Mrk 6 by Schurch et al. (2006).

5. SUMMARY AND CONCLUSIONS

We have carried out an extensive radio study with the VLA on the Seyfert 1.5 galaxy Mrk 6 and imaged a spectacular radio structure in the source. The radio emission occurs on three different spatial scales, from ~ 7.5 kpc bubbles to ~ 1.5 kpc bubbles and a ~ 1 kpc radio jet, all lying roughly orthogonal to each other. All the radio structures appear to originate from near the AGN core.

We have considered three models to explain the complex radio morphology of Mrk 6. In the first model, we have suggested that the bubble-like radio structures are the result of superwinds ejected by a nuclear starburst. However, recent Spitzer observations of Mrk 6 provide an upper limit to the star formation rate of $\sim 5.5 M_{\odot} \text{ yr}^{-1}$, an estimate lower by an order of magnitude than the SFR of $\sim 33 M_{\odot} \text{ yr}^{-1}$ derived assuming that the bubbles are a result of starburst winds energized by supernovae explosions. Thus, a starburst alone cannot meet the energy requirements for the creation of the bubbles in Mrk 6.

We have also considered a model wherein the bubbles are a result of diverted AGN-driven jets. The small-scale radio jet gets diverted and decelerated through its interaction with the surrounding interstellar medium, thereby depositing all its energy into the ISM in about 10^5 years. The energetics however, do not favour the AGN-driven single plasmon model proposed by Pedlar et al. (1985).

In the third model, we attribute the complex radio structure to be the result of an episodically-powered precessing jet that changes orientation. The attraction of this model is that it can naturally explain the complex radio morphology. It is also consistent with the energetics, the spectral index, and the polarization structure. Recent XMM-Newton X-ray observations of a variable absorbing gas column density could be inferred as in-keeping with the changing jet orientation in Mrk 6 which causes the jet to interact with the torus, thereby stirring up the gas/dust. Radio emission in this scenario is short-lived phenomenon in the lifetime of a Seyfert galaxy which results due to an accretion event. Further, possibly due to the smaller blackhole masses in Seyferts compared to typical radio galaxies, the spinning blackhole axis and consequently the radio jet axis is perturbed easily when accretion events take place, resulting in precessing jets and switches in orientation. Multi-wavelength

comprehensive radio studies of Seyfert galaxies would therefore reveal many more sources with similar complex radio structures as Mrk 6.

6. ACKNOWLEDGEMENTS

We thank the referee for insightful comments that improved the paper. We thank Prof. Martin Elvis for a stimulating discussion on the paper. The National Radio Astronomy Observatory is a facility of the National Science Foundation operated under cooperative agreement by Associated Universities, Inc. This research has made use of the NASA/IPAC Extragalactic Database (NED) which is operated by the Jet Propulsion Laboratory, California Institute of Technology, under contract with the National Aeronautics and Space Administration.

REFERENCES

- Balick B. 1987, *AJ*, 94, 671
- Baum S. A., O’Dea C. P., Dallacassa D., de Bruyn A. G., Pedlar A. 1993, *ApJ*, 419, 553
- Baum S. A., O’Dea C. P., de Koff S., Sparks W., Hayes J. J. E., Livio M., Golombek D. 1996, *ApJ*, 465, L5
- Begelman M. C., Blandford R. D., Rees M. J. 1980, *Nature*, 287, 307
- Bicknell G. V., Dopita M. A., Tsvetanov Z. I., Sutherland R. S. 1998, *ApJ*, 495, 680
- Blundell K. M., Mioduszewski A. J., Muxlow T. W. B., Podsiadlowski P., Rupen M. P. 2001, *ApJ*, 562, L79
- Bridle A. H., Chan K. L., Henriksen R. N. 1981, *JRASC*, 75, 69
- Bridle A. H., Perley R. A. 1984, *ARA&A*, 22, 319
- Buchanan C. L., Gallimore J. F., O’Dea C. P., Baum S. A., Axon D. J., Robinson A., Elitzur M., Elvis M. 2006, *AJ*, in press (astro-ph/0604222)
- Burbidge G. R. 1959, *ApJ*, 129, 849
- Capetti A., Axon D. J., Kukula M., Macchetto F., Pedlar A., Sparks W. B., Boksenberg A. 1995, *ApJ*, 454, L85

- Caproni A., Abraham Z. 2004a, MNRAS, 349, 1218
- Caproni A., Abraham Z. 2004b, in IAU Symposium Jet precession and its observational evidence: The cases of 3C 345 and 3C 120, 83
- Caproni A., Mosquera Cuesta H. J., Abraham Z. 2004, ApJ, 616, L99
- Clements E. D. 1981, MNRAS, 197, 829
- Colbert E. J. M., Baum S. A., Gallimore J. F., O’Dea C. P., Christensen J. A. 1996, ApJ, 467, 551
- Condon J. J. 1992, ARA&A, 30, 575
- Condon J. J., Cotton W. D., Broderick J. J. 2002, AJ, 124, 675
- Crocker M. M., Davis R. J., Spencer R. E., Eyres S. P. S., Bode M. F., Skopal A. 2002, MNRAS, 335, 1100
- Dahari O. 1985, AJ, 90, 1772
- de Bruyn A. G., Wilson A. S. 1976, A&A, 53, 93
- Dennett-Thorpe J., Scheuer P. A. G., Laing R. A., Bridle A. H., Pooley G. G., Reich W. 2002, MNRAS, 330, 609
- Dreher J. W., Feigelson E. D. 1984, Nature, 308, 43
- Duric N., Seaquist E. R. 1988, ApJ, 326, 574
- Dwarkadas V. V., Balick B. 1998, ApJ, 497, 267
- Gaensler B. M., Wallace B. J. 2003, ApJ, 594, 326
- Gallimore J. F., Axon D. J., O’Dea C. P., Baum S. A., Pedlar A. 2006, AJ, in press (astro-ph/0604219)
- Gallimore J. F., Baum S. A., O’Dea C. P., Pedlar A. 1996, ApJ, 458, 136
- Gallimore J. F., Holloway A. J., Pedlar A., Mundell C. G. 1998, A&A, 333, 13
- Genzel R., Weitzel L., Tacconi-Garman L. E., Blietz M., Cameron M., Krabbe A., Lutz D., Sternberg A. 1995, ApJ, 444, 129
- Heckman T. M., Armus L., Miley G. K. 1990, ApJS, 74, 833

- Heckman T. M., Lehnert M. D., Armus L. 1993, in *ASSL Vol. 188: The Environment and Evolution of Galaxies Galactic Superwinds*, 455
- Heckman T. M., Miley G. K., Balick B., van Breugel W. J. M., Butcher H. R. 1982, *ApJ*, 262, 529
- Hjellming R. M., Johnston K. J. 1981, *ApJ*, 246, L141
- Ho L. C., Filippenko A. V., Sargent W. L. W. 1997, *ApJ*, 487, 568
- Hunt L. K., Malkan M. A. 2004, *ApJ*, 616, 707
- Imai H., Obara K., Diamond P. J., Omodaka T., Sasao T. 2002, *Nature*, 417, 829
- Jaffe W. J., Perola G. C. 1973, *A&A*, 26, 423
- Kennicutt R. C. 1998, *ARA&A*, 36, 189
- Kinney A. L., Schmitt H. R., Clarke C. J., Pringle J. E., Ulvestad J. S., Antonucci R. R. J. 2000, *ApJ*, 537, 152
- Kukula M. J., Ghosh T., Pedlar A., Schilizzi R. T., Miley G. K., de Bruyn A. G., Saikia D. J. 1993, *MNRAS*, 264, 893
- Kukula M. J., Holloway A. J., Pedlar A., Meaburn J., Lopez J. A., Axon D. J., Schilizzi R. T., Baum S. A. 1996, *MNRAS*, 280, 1283
- Kukula M. J., Pedlar A., Baum S. A., O’Dea C. P. 1995, *MNRAS*, 276, 1262
- Lal D. V., Shastri P., Gabuzda D. C. 2004, *A&A*, 425, 99
- Lazendic J. S., Slane P. O., Gaensler B. M., Reynolds S. P., Plucinsky P. P., Hughes J. P. 2004, *ApJ*, 602, 271
- Lehto H. J., Valtonen M. J. 1996, *ApJ*, 460, 207
- Lim A. J. 2001, *MNRAS*, 327, 507
- Liu R., Pooley G. 1991, *MNRAS*, 253, 669
- Livio M., Pringle J. E. 1996, *ApJ*, 465, L55
- Livio M., Pringle J. E. 1997, *ApJ*, 486, 835
- Lopez J. A., Meaburn J., Palmer J. W. 1993, *ApJ*, 415, L135

- Maiolino R., Krabbe A., Thatte N., Genzel R. 1998, *ApJ*, 493, 650
- Mathews W. G., Brighenti F. 2003, *ARA&A*, 41, 191
- McConnell D., Carretti E., Subrahmanyan R. 2006, *AJ*, 131, 648
- McLure R. J., Dunlop J. S. 2001, *MNRAS*, 327, 199
- Meaburn J., Whitehead M. J., Pedlar A. 1989, *MNRAS*, 241, 1P
- Merritt D., Ekers R. D. 2002, *Science*, 297, 1310
- Merritt D., Milosavljević M. 2005, *Living Reviews in Relativity*, 8, 8
- Miranda L. F., Gómez Y., Anglada G., Torrelles J. M. 2001, *Nature*, 414, 284
- Morrison P., Sadun A. 1996, *MNRAS*, 278, 265
- Myers S. T., Spangler S. R. 1985, *ApJ*, 291, 52
- Nagar N. M., Wilson A. S., Mulchaey J. S., Gallimore J. F. 1999, *ApJS*, 120, 209
- Natarajan P., Pringle J. E. 1998, *ApJ*, 506, L97
- Nota A., Livio M., Clampin M., Schulte-Ladbeck R. 1995, *ApJ*, 448, 788
- O’Dea C. P. 1985, *ApJ*, 295, 80
- O’Dea C. P., Owen F. N. 1987, *ApJ*, 316, 95
- Pacholczyk A. G., Scott J. S. 1976, *ApJ*, 203, 313
- Padovani P., Rafanelli P. 1988, *A&A*, 205, 53
- Pedlar A., Kukula M. J., Longley D. P. T., Muxlow T. W. B., Axon D. J., Baum S., O’Dea C., Unger S. W. 1993, *MNRAS*, 263, 471
- Pedlar A., Unger S. W., Dyson J. E. 1985, *MNRAS*, 214, 463
- Peterson B. M., Ferrarese L., Gilbert K. M., Kaspi S., Malkan M. A., Maoz D., Merritt D., Netzer H., Onken C. A., Pogge R. W., Vestergaard M., Wandel A. 2004, *ApJ*, 613, 682
- Pfefferkorn F., Boller T., Rafanelli P. 2001, *A&A*, 368, 797
- Pringle J. 1997, *MNRAS*, 292, 136

- Pringle J. E. 1996, MNRAS, 281, 357
- Quillen A. C., Bland-Hawthorn J., Brookes M. H., Werner M. W., Smith J. D., Stern D., Keene J., Lawrence C. R. 2006, ApJ, 641, L29
- Raga A. C., Canto J., Biro S. 1993, MNRAS, 260, 163
- Rees M. J. 1978, Nature, 275, 516
- Rieke G. H., Loken K., Rieke M. J., Tamblyn P. 1993, ApJ, 412, 99
- Roy A. L., Norris R. P., Kesteven M. J., Troup E. R., Reynolds J. E. 1994, ApJ, 432, 496
- Sahai R., Le Mignant D., Sánchez Contreras C., Campbell R. D., Chaffee F. H. 2005, ApJ, 622, L53
- Sanders R. H. 1984, A&A, 140, 52
- Scheuer P. A. G., Feiler R. 1996, MNRAS, 282, 291
- Schmitt H. R., Antonucci R. R. J., Ulvestad J. S., Kinney A. L., Clarke C. J., Pringle J. E. 2001, ApJ, 555, 663
- Schmitt H. R., Kinney A. L. 2002, New Astronomy Review, 46, 231
- Schurch N. J., Griffiths R. E., Warwick R. S. 2006, ArXiv Astrophysics e-prints (astro-ph/0605451)
- Schwarz H. E., Monteiro H. 2004, in Meixner M., Kastner J. H., Balick B., Soker N., eds, ASP Conf. Ser. 313: Asymmetrical Planetary Nebulae III: Winds, Structure and the Thunderbird Binarities and Symbiotics in Asymmetrical Planetary Nebulae, 497
- Seaquist E. R., Odegard N. 1991, ApJ, 369, 320
- Shklovskii I. S. 1960, Soviet Astronomy, 4, 243
- Sillanpaa A., Haarala S., Valtonen M. J., Sundelius B., Byrd G. G. 1988, ApJ, 325, 628
- Simard-Normandin M., Kronberg P. P. 1980, ApJ, 242, 74
- Smith J. E., Robinson A., Alexander D. M., Young S., Axon D. J., Corbett E. A. 2004, MNRAS, 350, 140
- Soker N. 2004, ApJ, 612, 1060

- Soker N., Livio M. 1994, *ApJ*, 421, 219
- Terzian Y., Hajian A. R. 2000, in *ASP Conf. Ser. 199: Asymmetrical Planetary Nebulae II: From Origins to Microstructures Planetary Nebulae with the Hubble Space Telescope*, 33
- Thean A., Pedlar A., Kukula M. J., Baum S. A., O’Dea C. P. 2000, *MNRAS*, 314, 573
- Thean A. H. C., Gillibrand T. I., Pedlar A., Kukula M. J. 2001, *MNRAS*, 327, 369
- Ulvestad J. S., Roy A. L., Colbert E. J. M., Wilson A. S. 1998, *ApJ*, 496, 196
- Ulvestad J. S., Wilson A. S. 1984a, *ApJ*, 278, 544
- Ulvestad J. S., Wilson A. S. 1984b, *ApJ*, 285, 439
- Ulvestad J. S., Wrobel J. M., Roy A. L., Wilson A. S., Falcke H., Krichbaum T. P. 1999, *ApJ*, 517, L81
- van Breugel W., Fomalont E. B. 1984, *ApJ*, 282, L55
- Veilleux S., Cecil G., Bland-Hawthorn J., Tully R. B., Filippenko A. V., Sargent W. L. W. 1994, *ApJ*, 433, 48
- Velázquez P. F., Riera A., Raga A. C. 2004, *A&A*, 419, 991
- Wehrle A. E., Morris M. 1988, *AJ*, 95, 1689
- Whittle M., Silverman J. D., Rosario D. J., Wilson A. S., Nelson C. H. 2004, in *IAU Symposium No. 222 The Interplay among Black Holes, Stars and ISM in Galactic Nuclei*, 299